Behavior of external beam-column connection under Earthquake loading

Ahmed Hamed [1], Aymen Abo Beah [2], Ahmed Ghallab [3]

Abstract— The beam-column joint is a very critical part of reinforced concrete framed structures. Joints ensure continuity of a structure and transfer forces that are present at the ends of the members. In reinforced concrete structures, failure in a beam often occurs at the beam-column joint, making the joint one of the most critical sections of the structure system. Several factors can affect the joint behavior such as joint geometry, amount and detailing of reinforcement, relative stiff ness between beam and column, concrete strength, loading pattern, and the column acting axial load etc. For better understating the behavior of beam column joints under seismic loading, three different factors; spacing between stirrups inside joint, shape of branches, and axial normal force were analytically studied using a non-linear finite element analysis software program (ABAQUS). Analytical models consist of five specimens of beam column Joints with different spacing between inside joints with the same reinforcement to study the effect of spacing between stirrups inside joint. Also consist of three specimens of beam-column Joints, with different shape of branches with the same reinforcement to study the effect of shape of stirrups. Another three specimens of beam-column Joints, with different axial normal force with the same reinforcement to study the effect of normal force. All models were constructed from normal strength concrete (with f'c= 46.2 MPa) and tested under same test setup conditions under fixed load at the column and monotonic loading at beam end. Parameters such as ultimate load, displacement, energy dissipation capacity and crack behavior of concrete were examined. The results show that all joints exhibited the same failure mode in joint for spacing between stirrups in joint effect. Joints with low spacing between stirrups in joints were higher than the joints with high spacing between stirrups inside joint in dissipation energy and ductility. For shape of branches, the results showed that increasing branches perpendicular to loading plane cause increasing dissipation energy and ductility. For normal force, the results showed that increasing normal force cause increasing ultimate load, dissipation energy and reducing ductility.

Index Terms— Beam column joint, Reinforced concrete joint, monotonic loading, Analytical modelling, Abaqus modelling, Numerical modelling, Parametric study, Exterior connection.

1 Introduction

During earthquake, beam-column joints in frame structure play an important role in resisting lateral load. Joints should be well designed and detailed to satisfy both the strength and ductility [1], [2],[3].

Ductility and strength of the beam-column joints depend on several factors such as transverse reinforcement, longitudinal reinforcement, concrete strength, dimensions of joint and loading pattern, ... etc. To improve the strength and ductility of beam-column joint longitudinal and horizontal reinforcement are required within the joint. This results in reinforcement congestion and construction difficulties.

To understand the behavior of beam-column connection under lateral load, many researches were conducted. Dehkordil et al. [10] tested six beam-column connections subjected to lateral cyclic quasi-static loading under constant column axial load ~~of~~ equals 160 kN to investigate the effects of concrete compressive strength on the seismic performance of beam-column joints. . They concluded that that utilizing high-strength concrete (HSC) was able to improve the cumulative energy dissipation and pinching width ratio by a maximum of 30% at a drift ratio of 4.5%.

Wong and Kuang [11] tested three reinforced concrete exterior beam–column joints with different intermediate longitudinal reinforcement in column under reversed cyclic loading. They stated that increasing the intermediate longitudinal steel ratio from 0 to 0.35% and 0.7%, the shear strength increased by 24% and 33%.

To investigate the effect of column longitudinal reinforcement and beam longitudinal reinforcement on the displacement ductility and curvature ductility, and based on results of non-linear Finite Element analysis, Dabiri et al [12] concluded that by increasing the ratio of column reinforcement, displacement ductility increases while curvature ductility fluctuates. Also, increasing beam longitudinal reinforcement both the displacement ductility and curvature ductility decreases.

Wong and Kuang [13], tested full-scale reinforced concrete exterior beam-column joints with no seismic design under reversed cyclic-load to study the seismic behavior of the joints and the effectiveness of adding horizontal stirrups in joint core on the seismic performance and shear strength of the joints. they concluded that the shear strength increases as the joint core stirrup ratio increases.

For better understanding the behavior of reinforced concrete beam column joints under earthquake load, effect of three different factors; spacing between stirrups inside joint, number of

- *(1) Teaching assistant at faculty of engineering, Badr University in Cairo and MSc Candidate at faculty of engineering, Ain Shams University.*
- *(2) Assistant Professor at structural department at faculty of engineering, Ain Shams University.*
- *(3) Professor of Concrete structures at faculty of engineering, Ain Shams University.*

branches, and normal force are studied. Nine beams were analytically modeled and tested till failure. Results of these beams are shown in this paper.

2 FINITE ELEMENT MODEL

Finite element analysis (FEA) is an extremely useful tool for numerically approximating physical structures that are too complex for regular analytical solutions. A finite element models were performed to simulate the behavior of the tested specimens using Abaqus/CAE (Complete Abaqus Environment) [4]. Details of the analytical model are followed.

2.1 Element Types

Two-node truss element (T3D2) with 3 degrees of freedom in every node was utilized to model steel reinforcement bars. To generate concrete column and beam 8-node brick element (C3D8) with three degrees of freedom in every node was considered.

2.2 Concrete modelling

2.2.1 Concrete damage plasticity

Concrete damage plasticity (CDP) is used as the governing concrete material plasticity model over the whole geometry of the specimens. The model is a plasticity-based model which is developed using concepts of continuum damage mechanics and the application of scalar damaged elasticity in combination with isotropic tensile and compressive plasticity to properly represent the inelastic behavior of concrete (Lubliner et al.) [5]. The main two failure mechanisms of the concrete material are tensile cracking and compressive crushing according to fundamental assumptions of damage plasticity model. The evolution of the yield (or failure) surface and the degradation of elastic stiffness in damage plasticity model are controlled by two hardening variables which are tensile and compressive equivalent plastic strains ($\dot{\varepsilon}_t^{pl}$ and $\dot{\varepsilon}_c^{pl}$). Increasing values of the hardening variables leads to the initiation of micro-cracking and progressive propagation of cracks or the occurrence of crushing in the concrete material.

2.2.2 Damage parameters

Damage is defined for both uniaxial tension and compression during softening procedure in concrete damage plasticity model. Damage in compression occurs just after reaching to the maximum uniaxial compressive strength. The degradation of elastic stiffness in softening regime is characterized by two damage variables, dt and dc corresponding to tensile and compressive damage, respectively.

According to Jankowiak and Lodygowski [6] , the scaler damage parameters in compression dc and in tension dt are only included in the model in the descending portion of the stress–strain curve, according to Eqs. (1) and (2) and as shown in the Figs. 1 and 2.

$$dc=1-\frac{fc}{f`c} \quad (1)$$

$$dt=1-\frac{\sigma t}{ft} \quad (2)$$

Wheref'c is the cylinder compressive strength of concrete, fc is compressive stress, ft is concrete tensile strength which has a value of $0.62\sqrt{f`c}$ according to the ACI 318-19 [1], σt is tensile stress.

In ABAQUS, the user provides the damage parameter and inelastic strain (dc and $\dot{\varepsilon}_c^{in}$) data in compression. In return, ABAQUS will internally compute the plastic strain ($\dot{\varepsilon}_c^{pl}$) according to Eqs. (3) and (4) and as shown in the Fig. 1.
Where ε_c is total strain corresponding stress fc, $\dot{\varepsilon}_{oc}^{el}$ is elastic strain and E_o is the initial elastic modulus, which is taken as $4700\sqrt{f`c}$ Mpa according to the ACI 318-19[1].

$$\dot{\varepsilon}_c^{pl} = \dot{\varepsilon}_c^{in} - \frac{dc}{(1-dc)}\frac{fc}{Eo} \quad (3)$$

$$\dot{\varepsilon}_c^{in} = \varepsilon_c - \dot{\varepsilon}_{oc}^{el}, \quad (4)$$

where $\dot{\varepsilon}_{oc}^{el} = \frac{fc}{Eo}$

Similarly, the user provides the damage parameter and cracking strain (dt and $\dot{\varepsilon}_t^{ck}$) data in tension. In return, ABAQUS will internally compute the plastic strain ($\dot{\varepsilon}_t^{pl}$) according to Eqs. (5) and (6) and as shown in the Fig. 2.
where ε_t is total strain corresponding stress σt and $\dot{\varepsilon}_{ot}^{el}$ is elastic strain.

$$\dot{\varepsilon}_t^{pl} = \dot{\varepsilon}_t^{in} - \frac{dt}{(1-dt)}\frac{\sigma t}{Eo} \quad (5)$$

$$\dot{\varepsilon}_t^{ck} = \varepsilon_t - \dot{\varepsilon}_{ot}^{el}, \quad (6)$$

where $\dot{\varepsilon}_{ot}^{el} = \frac{\sigma t}{Eo}$

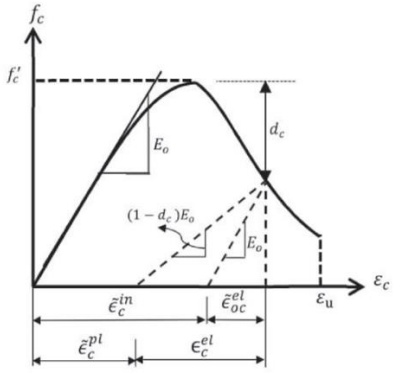

Fig. 1. Definition of concrete behavior in compression for CDP model.

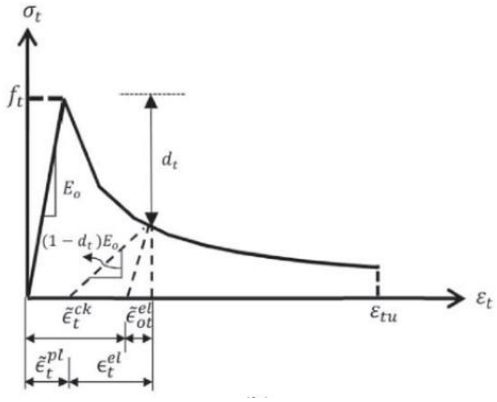

Fig. 2. Definition of concrete behavior in tension for CDP model.

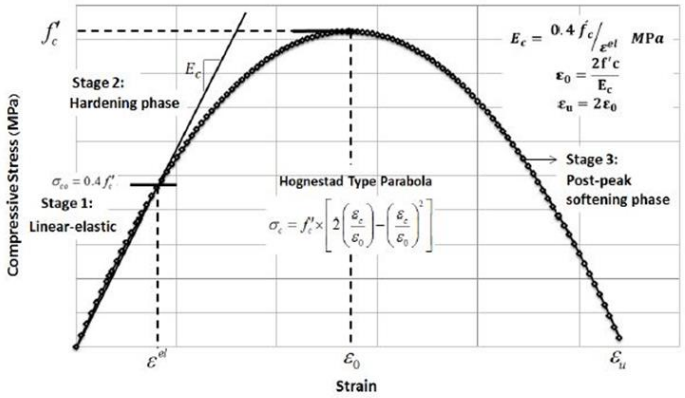

Fig. 3. stress-strain curve in compression for CDP model.

2.2.3 Plasticity parameters

Table 1 present the plasticity parameter needed to be defined in ABAQUS, these parameters are chosen based on the recommendations of Simulia [4] and Najafgholipour et al. [14].

TABLE 1
PLASTICITY PARAMETERS IN ABAQUS

dilation angle	eccentricity	Kc	σ_{bo}/σ_{co}	Viscosity parameter
35	0.1	0.667	1.16	0.005

2.2.4 Concrete material properties

Uniaxial stress-strain behavior of concrete in compression is simulated utilizing Hognestad type parabola (Hognestad)[7]. The uniaxial stress-strain behavior of concrete can be categorized into three main domains. The first one represents the linear-elastic branch which continues to reach the stress level of σ_{co} that is taken as $\sigma_{co}=0.4f`c$. The second stage shows the hardening part of the concrete uniaxial compressive stress-strain behavior which describes the ascending branch of the stress–strain relationship reaching to the peak load at the corresponding strain level $\varepsilon o=2f`c/Ec$. The last part of concrete uniaxial compressive stress-strain relationship attributes to the post-peak softening behavior and therefore represents the initiation and progression of compressive damage in the concrete material until the ultimate compressive strain εu. Fig. 3 shows the compressive stress-strain behavior of concrete which is introduced to the presented numerical model.

Uniaxial stress-strain behavior of concrete in tension is simulated utilizing Aslani and Jowkarmeimandi [15] and is shown in Fig. 2. The ascending part follows a linear relation until it reaches the concrete tensile strength ft which has a value of $ft=0.62\sqrt{f`c}$ according to the ACI 318-19[1] and the softening behavior after cracking is expressed by Eq. (7), in which σ_t is the stress corresponding to strain ε_t, and ε_{to}, is the first cracking strain corresponding to is concrete tensile strength ft.

$$\sigma t=ft\left(\frac{\varepsilon to}{\varepsilon t}\right)^{0.85} \quad (7)$$

2.2.5 Reinforcement modeling

Stress-strain relation of steel bars proposed by (Yun and Gardner) [8] is used in this study. This relation is divided to three parts, bilinear and nonlinear hardening material as shown in Fig. 4. The relation between stress-strain at each stage is as follows;

$$f(\varepsilon)=\begin{cases} Es*\varepsilon, & \text{for } \varepsilon\le\varepsilon_y \\ fy, & \text{for } \varepsilon_y<\varepsilon\le\varepsilon_{sh} \\ fy+(fu-fy)\left\{0.4\left(\frac{\varepsilon-\varepsilon sh}{\varepsilon u-\varepsilon sh}\right)+2\left(\frac{\varepsilon-\varepsilon sh}{\varepsilon u-\varepsilon sh}\right)/\left[1+400\left(\frac{\varepsilon-\varepsilon sh}{\varepsilon u-\varepsilon sh}\right)^5\right]^{1/5}\right., & \text{for } \varepsilon_{sh}<\varepsilon\le\varepsilon_u \end{cases} \quad (8)$$

$$\varepsilon_u=0.6\left(1-\frac{fy}{fu}\right), \qquad \varepsilon u\ge 0.06 \quad (9)$$

$$\varepsilon_{sh}=0.1\frac{fy}{fu}-0.55, \qquad 0.015\le\varepsilon u\le 0.03 \quad (10)$$

Where f(ε) is the steel stress corresponding to steel strain (ε), fy is yield strength of steel, fu is ultimate strength of steel, ε_{sh} is steel strain hardening, ε_u is ultimate strain and Es is steel modulus of elasticity is considered as 200GPa.

The steel reinforcement is modeled in ABAQUS as one-

dimensional bars embedded inside the concrete elements using the embedment constraint, and a perfect bond between the concrete and steel reinforcement is considered.

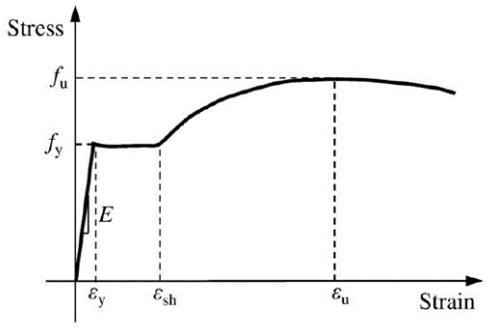

Fig. 4. stress-strain curve for steel

3 VERIFICATION OF NUMERICAL MODELS WITH EXPERIMENTAL RESULTS

To verify the suggested model, results of an experimental test carried by clyde et al. [9] are used. Model with the same dimensions and reinforcement details as those of the actual exterior connection test specimens is prepared. Details regarding specimens dimension and reinforcement are shown in Fig. 5.

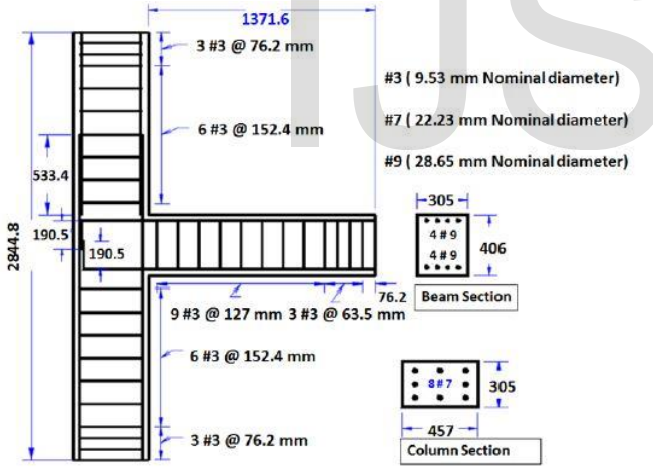

Fig. 5. Specimen details

3.1 Meshing

A uniform mesh with size of 50 mm is chosen for the concrete elements over the whole geometry in exterior connection specimen as shown in Figure. The same size for reinforcement mesh is also adopted for steel bars. Concrete meshing and reinforcement details are shown in Figs. 6 and 7.

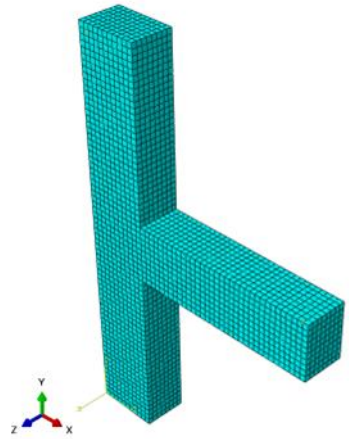

Fig. 6. Concrete element mesh of exterior connection.

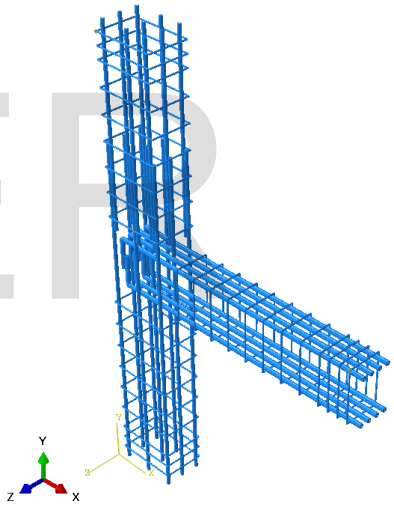

Fig. 7. Reinforcement details of exterior connection

3.2 Model Geometry and boundary conditions

Restraints were defined at both top and bottom surfaces of the specimen's column in the exterior test specimen according to boundary conditions addressed in the test setup. Details regarding to the geometry and boundary conditions of the both RC exterior beam-column connections which are applied to the finite element models are illustrated in Fig. 8. Loading is introduced to the model in two steps. The first step is the column compressive axial load=0.1 f`c and applied to the column top surface which remained constant during the analysis procedure. The second step is monotonic lateral loading at the beam's end surface. Loading is shown in Fig. 9.

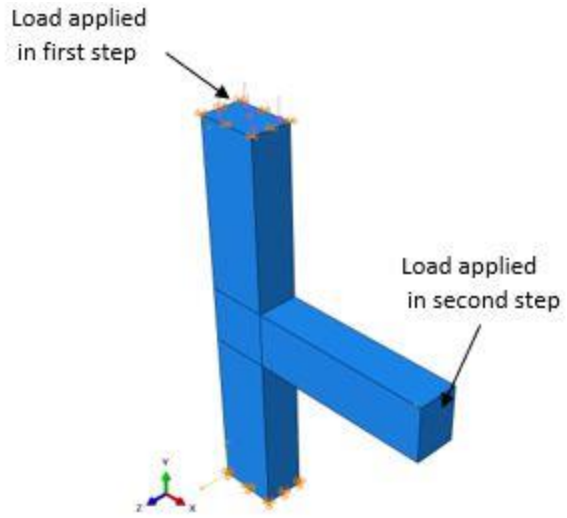

Fig. 8. loading of exterior connection

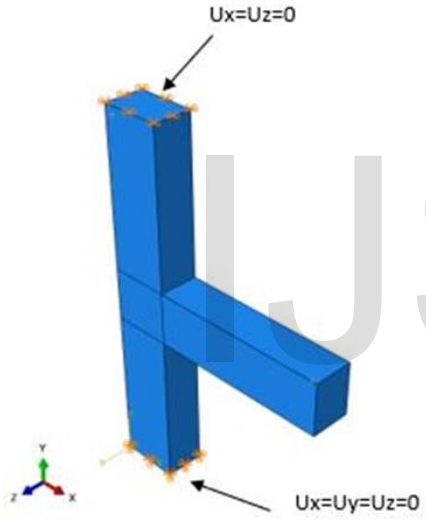

Fig. 9. boundary conditions of exterior connection

3.3 Material properties

The measured uniaxial concrete compressive strength of the test specimens, the yield strength and the ultimate tensile strength of reinforcement used in the tests, are reported in Table 2.

TABLE 2
MATERIAL PROPERTIES OF THE TEST SPECIMENS.

Concrete compressive strength f`c(Mpa)	Reinforcement type	Yield strength Fy (MPa)	Ultimate tensile strength Fu (MPa)
46.2	Beam longitudinal	454.4	746
	Column longitudinal	469.5	741.9
	Stirrups	427.5	654.3

3.4 Results

The FEA results of the RC beam-column connections subjected to lateral loading is presented in terms of force-displacement curves, ultimate loads and displacements.

The load versus deflection curve for both analytical and experimental results for specimens (are presented in Fig.11) while Table 3 shows the maximum load and the corresponding maximum displacement from the experimental work and those obtained from the finite element. A good agreement between the experimental and theoretical results are shown from both curves and results.

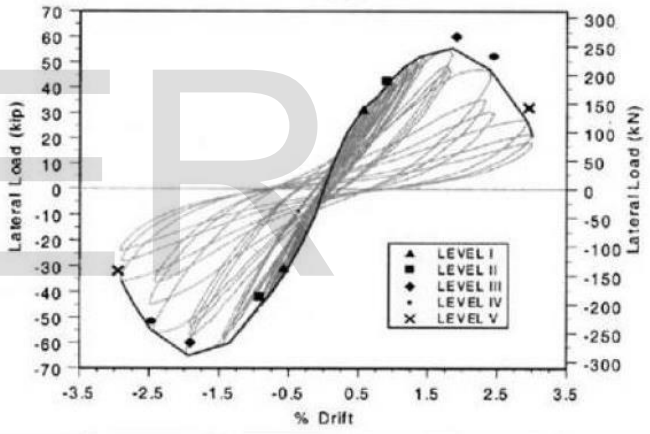

Fig. 10. Test results of exterior specimen obtained by Clyde et al. experimental study.

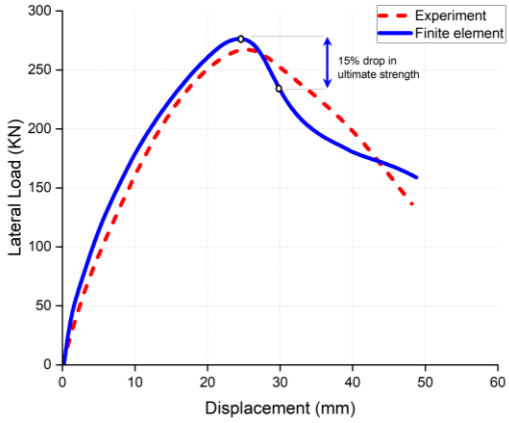

Fig. 11. The load versus deflection curve for both analytical and experimental results

TABLE 3

COMPARISON BETWEEN FINITE ELEMENT RESULTS AND EXPERIMENTAL RESULTS

Experimental results		Finite element analysis		Error(%)	
Peak lateral load (kN)	Displacement at peak lateral load (mm)	Peak lateral load (kN)	Displacement at peak lateral load (mm)	Peak lateral load	Displacement at peak lateral load
267.26	25.33	276.33	24.46	3.28	3.43

4 PARAMETRIC STUDY

Based on validation of FE model using experimental results of Clyde et al. as discussed above, the calibrated FE model is used to extend the research work to study the effect of the following factors on the behavior of exterior beam – column joint:

- effect of spacing between stirrups inside the joint,
- shape of stirrups
- normal force value.

Figure 12 shows the Specimen dimensions and details while table 4 summaries the configuration of FE models and variables of the parametric study. The analysis was performed for nine exterior beam column connection under monotonic loading and Specimen (J4) was considered as control specimen.

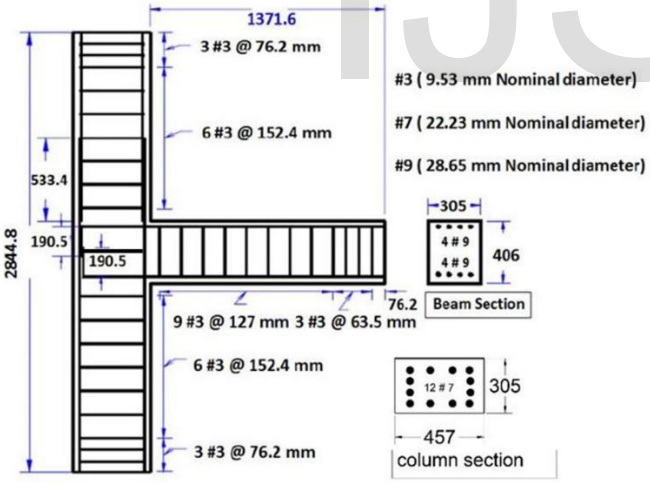

Fig. 12. Specimen dimensions and details of Exterior beam-column connection

TABLE 4

CONFIGURATION OF FE MODELS AND VARIABLES OF THE PARAMETRIC STUDY

Studied Factor	No. of specimen	spacing between stirrups (mm)	No of branches	Normal Force	Column dimensions (mm)	Beam dimensions (mm)
Spacing between stirrups inside joints (Group A)	J1	200	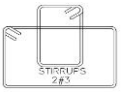	0.1 F'c	305 x 457	305 x 406
	J2	150	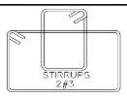	0.1 F'c	305 x 457	305 x 406
	J3	100	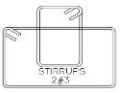	0.1 F'c	305 x 457	305 x 406
	J4	75	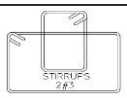	0.1 F'c	305 x 457	305 x 406
	J5	50	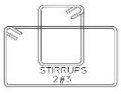	0.1 F'c	305 x 457	305 x 406
Shape of stirrups (Group B)	s1	75	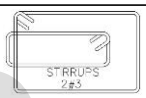	0.1 F'c	305 x 457	305 x 406
	s2	75		0.1 F'c	305 x 457	305 x 406
Normal force (Group C)	P1	75	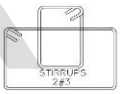	0.45 F'c	305 x 457	305 x 406
	P2	75	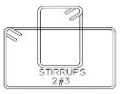	0.65 F'c	305 x 457	305 x 406

5 RESULTS AND DISCUSSION

The results of analytical model are presented in this section. The test results during the test are presented and evaluated in different forms such as crack pattern and failure mode, load-displacement curves, cracking and ultimate loads, displacement ductility and dissipation energy.

5.1 Effect of spacing between stirrups inside joint

5.1.1 Crack pattern and failure mode

For group A: the first crack was at beam then occurred inside the joint. As shown in Fig.13, the cracks propagated diagonally.it was noticed the decreasing spacing between stirrups led to decrease propagation of cracks in joint. This observation confirmed that role of the joint stirrups to act as a tension tie The failure was at joint due to shear.

Fig. 13. Crack pattern for Group A

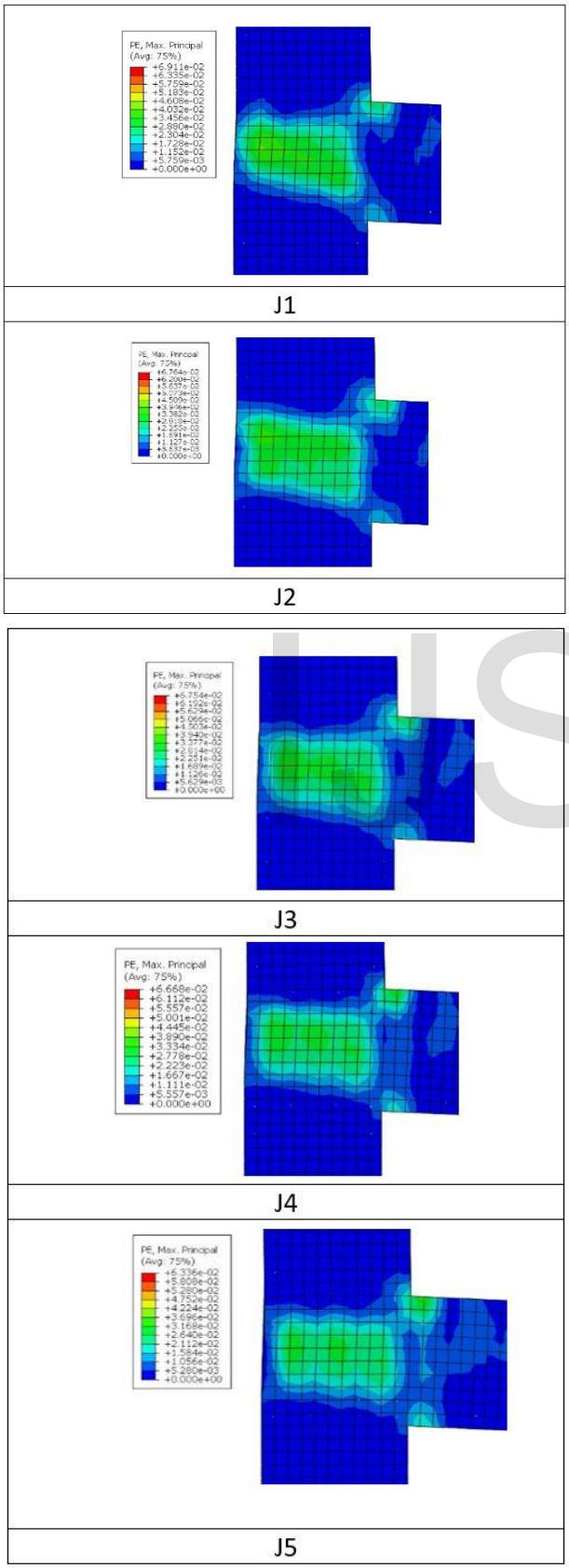

5.1.2 Load displacement curve

For the load–deflection curves of group A. The results as shown in Fig.15, indicate that the joint performance in terms of joint dissipation energy is significantly affected by spacing between stirrups inside joint.

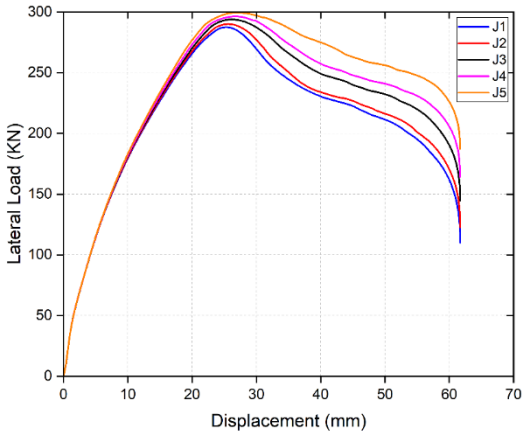

Fig. 14. the load–deflection curves for Group A

5.1.3 Cracking and ultimate loads

As shown in table 5 For Group A (J1 to J5), the first crack in the beam was flexure crack at the same displacement and load; on the other hand, the first crack in Joint delay from J1 up to J5. For cracking displacement increased by 0.54%, 1.25%, 8.44% and 14.66% for J2, J3, J4 and J5 respectively compared with J1. For cracking load increased by 0.122%, 2.27%, 6.31 and 10.9% for J2, J3, J4 and J5 respectively compared with J1. After first crack, cracks propagated diagonal.

Also, decreasing spacing between stirrups cause increasing in loading capacity by 0.87 %, 2.14%, 2.98% and 4.02% for J2, J3, J4 and J5 respectively compared with case of J1 and increasing in displacement capacity by 1.25%, 3.33%, 5.46% and 6.58% for J2, J3, J4 and J5 respectively compared with case of J1.

TABLE 5

CRACKING, AND ULTIMATE LOAD FOR GROUP A

Number of Joint	First Crack				Peak		Failure place
	Beam		Joint				
	Disp.(mm)	Load(KN)	Disp.(mm)	Load(KN)	Peak Disp. (mm)	Peak Load (KN)	
J 1	0.93	31.69	5.53	122.65	25.28	287.5	joint
J 2	0.93	31.71	5.56	122.8	25.6	290.03	joint
J 3	0.93	31.72	5.6	125.5	26.15	293.8	joint
J 4	0.93	31.74	6.04	130.91	26.74	296.33	joint
J 5	0.93	31.76	6.48	137.67	27.06	299.55	joint

5.1.4 Displacement ductility

Ductility is the ability of a reinforced member to sustain large inelastic deformations without excessive strength deterioration. It can be quantified using several measures such as curvature ductility factor, drift index, and displacement ductility factor. To evaluating the performance of the tested specimens, displacement ductility factor μΔ was used as a convenient measure of ductility. It was calculated as follows:

$$\mu\Delta = \Delta 85/\Delta y \quad (11)$$

Where:

Δy the yield displacement

Δ85 the displacement at 85% of the ultimate load

As shown in Fig. 15, the decrease of spacing between stirrups in joint caused an increase in ductility by 0.84%, 1.26%, 1.67% and 10.94% for J2, J3, J4, J5 respectively compared with case of J1.

Fig. 15. Displacement Ductility (μ) for group A

5.1.5 Dissipation Energy

The ability to dissipate the inelastic deformation energy is a significant factor for evaluating the performance of column beam Joints subjected to lateral loads. The energy dissipated by the specimen defined as the area enclosed within the load-displacement curve. The total energy dissipated was then estimated as the sum of the cumulative dissipated energy during test.

As shown in Fig.16, the decrease of spacing between stirrups in joint caused an increase in dissipation energy by 3.32%, 16.46%, 24.63% and 38.74% for J2, J3, J4, J5 respectively compared with case of J1.

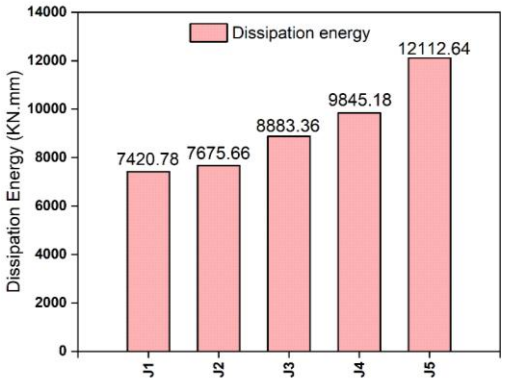

Fig. 16. Dissipation Energy for J1 to J5

5.2 Effect of shape of stirrups

5.2.1 Crack pattern and failure mode

For group B: the first crack was at beam then occurred inside the joint. As shown in Fig.17, The cracks propagated diagonally. It was noticed that cracks propagation was less in case of cross ties perpendicular to plane of loading. This observation confirmed that increasing cross ties perpendicular to plane of loading is more efficient to stirrups to act as tension tie The failure was at joint due to shear.

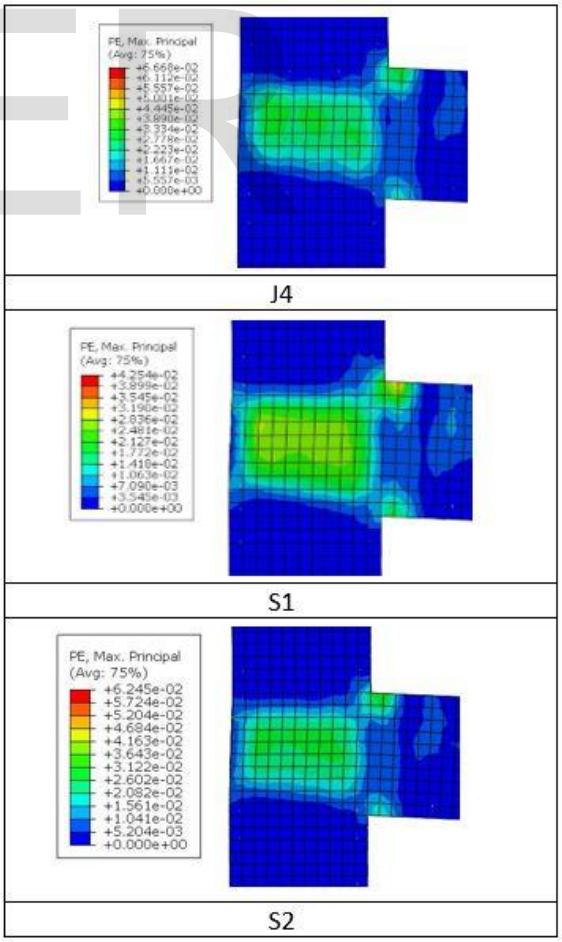

Fig. 17. Crack pattern for Group B

5.2.2 Load displacement curve

For the load–deflection curves of group B. As shown in Fig.18, the results indicate that the joint performance in terms of joint dissipation energy is slightly affected by Changing shape of stirrups in joint. without changing total area of the stirrups.

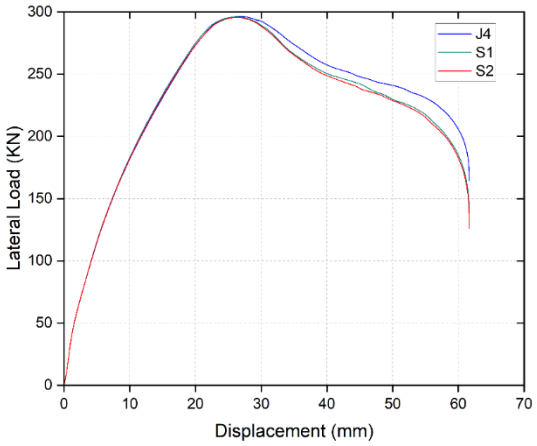

Fig. 18. the load–deflection curves for Group B

5.2.3 Cracking and ultimate loads

As shown in Table 6, for Specimens J4, S1 and S2, the first crack in the beam was flexure crack at the same displacement and load; on the other hand, the first crack in Joint delay from J4 up to S2. For cracking displacement increased by 2.1% and 5.625% for S1 and S2 respectively compared with J4. For cracking load increased by 2.1% and 4.2 % respectively compared with J4. After first crack, cracks propagated diagonal. The failure was at joint for all specimens.

Also, changing shape of stirrups without change total area of stirrups for S1 and S2 cause decreasing in load capacity by 1.34 % and 1.55% respectively compared with case of J4 but displacement capacity almost the same for all specimens.

TABLE 6

CRACKING, AND ULTIMATE LOAD FOR GROUP A

Number of Joint	First Crack				Peak		Failure place
	Beam		Joint				
	Disp.(mm)	Load(KN)	Disp.(mm)	Load(KN)	Peak Disp. (mm)	Peak Load (KN)	
J 4	0.93	31.74	6.04	130.91	26.74	296.33	joint
S1	0.93	31.79	6.17	133.72	26.38	296.15	joint
S2	0.93	31.78	6.4	136.68	26.324	295.55	joint

5.2.4 Displacement ductility

The results show that changing shape of stirrups without change total area of stirrups for S1 and S2 caused a decrease in ductility by 6.19%, 8.3 for S1 and S2 respectively compared with case of J4. as shown in Fig. 19.

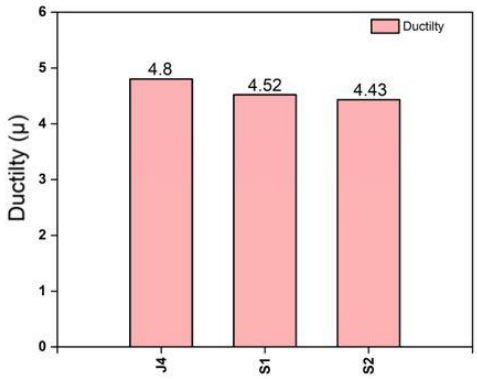

Fig. 19. Displacement Ductility (μ) for group B

5.2.5 Dissipation Energy

The change shape of stirrups without changing total area of stirrups caused a decrease in dissipation energy by 11.04% and 13.26% for S1, S2, respectively compared with case of J4 as shown in figure 20.

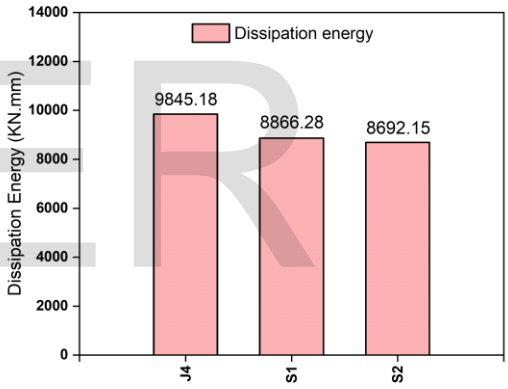

Fig. 20. Dissipation Energy for group B

5.3 Effect of axial normal force

5.3.1 Crack pattern and failure mode

For group C: the first crack was at corners of joint then occurred in beam. The cracks in joints propagated diagonally. It was noticed that increasing axial normal force led to increase the inclination of joint cracks. This observation because of the higher axial normal load results in the formation of a steeper diagonal strut. and the failure was at beam column face as shown in Fig. 21.

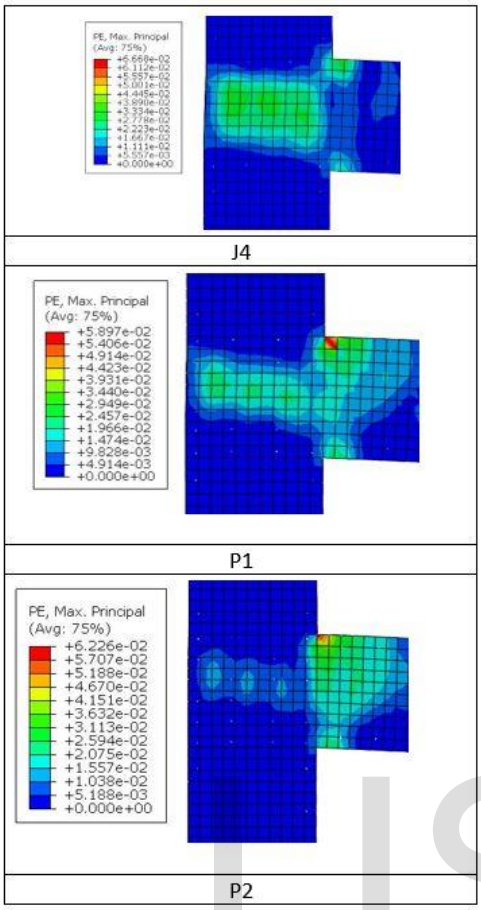

Fig. 21. Crack pattern for Group C

5.3.2 Load displacement curve

For the load–deflection curves of group C. As shown in Fig.22, The results indicate that the joint performance in terms of joint strength , deformation capacity and dissipation energy is significantly affected by Changing the axial normal force value.

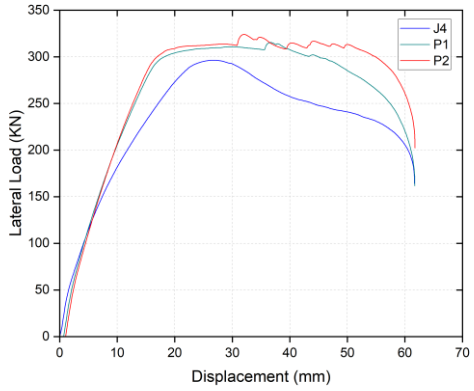

Fig. 22. the load–deflection curves for Group C

5.3.3 Cracking and ultimate loads

As shown in Table 7, For Specimens J4, P1 and P2, the first crack in corners of joint occurred at axial load 2175.44 kN; on the other hand, and the first crack in beam occurred at axial load 2234.78 kN. Cracks in P1 and P2 occurred before J4 due to high axial load. After first crack, cracks propagated diagonal.

Also, increasing normal force on column for P1 and P2 cause increasing in load capacity by 6.43 % and 9.34% respectively compared with case of J4. Else increasing in displacement capacity by 37.21% and 19.67% for P1 and P2 respectively compared with case of J4. which confirmed to the fact that the increasing axial normal load confined the joint against shear failure.

TABLE 7
CRACKING, AND ULTIMATE LOAD FOR GROUP A

Number of Joint	First Crack				Peak		Failure place
	Beam		Joint				
	Disp.(mm)	Load(KN)	Disp.(mm)	Load(KN)	Peak Disp. (mm)	Peak Load (KN)	
J 4	0.93	31.74	6.04	130.91	26.74	296.33	joint
P1	at axial load 2234.78 KN		at axial load 2175.44 KN		36.69	315.4	beam column face
P2	at axial load 2234.78 KN		at axial load 2175.44 KN		32	324.03	beam column face

5.3.4 Displacement ductility

As shown in fig. 23, the results show that decreasing in ductility with an increase in axial load on column by 16.7%. This effect was more pronounced for column axial loads of 0.45 f'cAg for P1 compared with the corresponding case of column axial loads of 0.1 f 'cAg for J4.

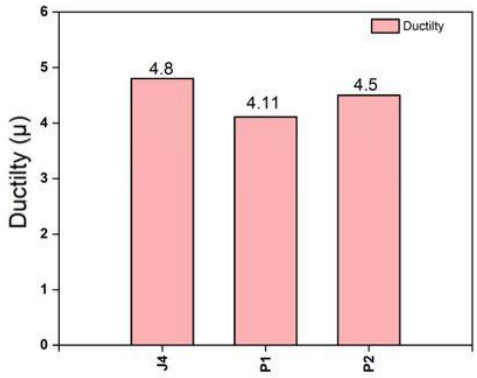

Fig. 23. Displacement Ductility (μ) for group C

5.3.5 Dissipation Energy

The results show that increasing normal force on column for P1 and P2 caused a increase in dissipation energy by 30.49% and 37.89% for P1, P2, respectively compared with case of J4 as shown in figure 24.

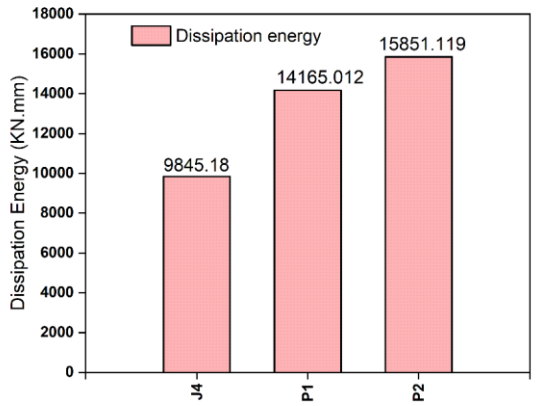

Fig. 24. Dissipation Energy for group C

6 CONCLUSION

Nine beams were analytically modeled and tested till failure. To understand the behavior of reinforced concrete beam column joints under earthquake load, effect of three different factors; spacing between stirrups inside joint, number of branches, and axial normal force are studied, and It was concluded that:

- Decreasing spacing between stirrups cause delaying in first crack in joint. That clarified the role of the spacing between joint stirrups in crack control.
- Decreasing spacing between stirrups cause increasing in ductility and dissipation energy.
- Increasing cross ties perpendicular to plane of loading cause increasing in ductility and dissipation energy.
- Increasing column compression load results in delaying the initiation of first shear crack and the failure was at beam column interface.
- Increasing column compression load from (0.1 f`c Ag to 0.65 f`c Ag) results in increasing dissipation energy by 37.89%.
- For the studied joints, where the joint failure was due to shear failure, but when increasing the column axial load resulted in increasing the beam tip ultimate load and failure was at beam column face.

7 REFRENCES

[1] ACI 318-19 Committee. Building code requirements for structural concrete (ACI 318-19) and commentary. American Concrete Institute, Farmington Hills, Michigan, 2019.

[2] ACI-ASCE Committee 352R-02, "Recommendations for Design of Beam-Column Connections in Monolithic Reinforced Concrete Structures".

[3] Egyptian Code for Design and Construction of Reinforced Concrete Structures, (ECP 203-2020).

[4] Simulia (2016). Abaqus Analysis User's Guide. Dassault Systems Simulia Corp.

[5] Lubliner, J., Oliver, J., Oller, S. and Oñate, E. (1989). "A plastic-damage model for concrete.." International Journal of Solids and Structures 25: 299-329.

[6] Jankowiak T and Lodygowski T. (2005). "Identification of parameters of concrete damage plasticity constitutive model " Foundations of Civil and Environmental Engineering ,6(1), PP. 53–69

[7] Hognestad, E. (1951). A study of combined bending and axial load in reinforced concrete members, University of Illinois, engineering experiment station, bulletin series No.399.

[8] Yun, X. and Gardner, L. (2017). "Stress-strain curves for hot-rolled steels" Journal of Constructional Steel Research 133 , PP. 36–46.

[9] Clyde, M. E. C., Pantelides, C. P. and Reaveley, L. D. (2002) "Performance-Based Evaluation of Exterior Reinforced Concrete Building Joints for Seismic Excitation" Earthquake Spectra, Volume 18, No. 3, PP. 449–480, August 2002, Earthquake Engineering Research Institute.

[10] Dehkordi1 S., Mostofinejad D., Alaee p. (2019). "Effects of high-strength reinforcing bars and concrete on seismic behavior of RC beam-column joints.", Engineering Structures 183 (2019) 702–71910

[11] Wong, H. F. and Kuang, J. S. (2008). "Effects of beam–column depth ratio on joint seismic behavior. " Proceedings of the Institution of Civil Engineers Structures & Buildings 161 April 2008 Issue SB2 PP. 91–101.

[12] Dabiri, H. F. H., Kaviani, A. and Kheyroddin A.(2020)."Influence of reinforcement on the performance of non-seismically detailed RC beam-column joints." Journal of Building Engineering 7 March (2020).

[13] Wong, H. F. and Kuang, J. S.(2011). "Effectiveness of Horizontal Stirrups in Joint Core for Exterior Beam-Column Joints with Nonseismic Design" Procedia Engineering 14 3301–3307.

[14] Najafgholipour M. A., S.M. Dehghan M. A., Dooshabi A. and Niroomandi A.(2017). "Finite Element Analysis of Reinforced Concrete Beam-Column Connections with Governing Joint Shear Failure Mode", Latin American Journal of Solids and Structures 14 PP. 1200-1225.

[15] Aslani F, Jowkarmeimandi R.(2012). Stress–strain model for concrete under cyclic loading. Mag Concr Res; 64(8):673–85.